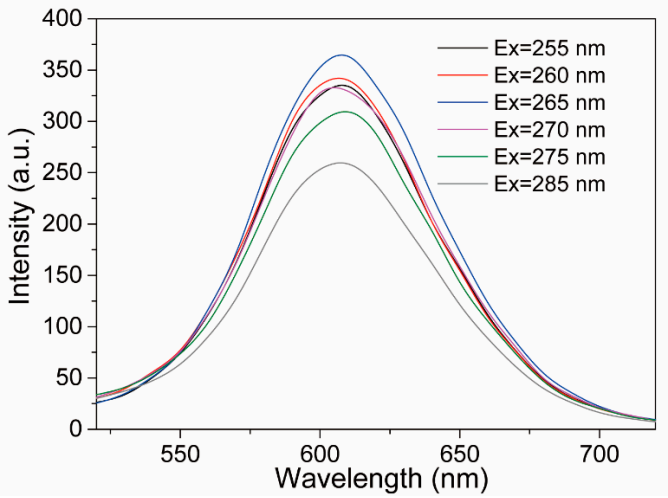

Figure S1. Fluorescence emission spectra of MUA-AuNCs at different excitation wavelengths.

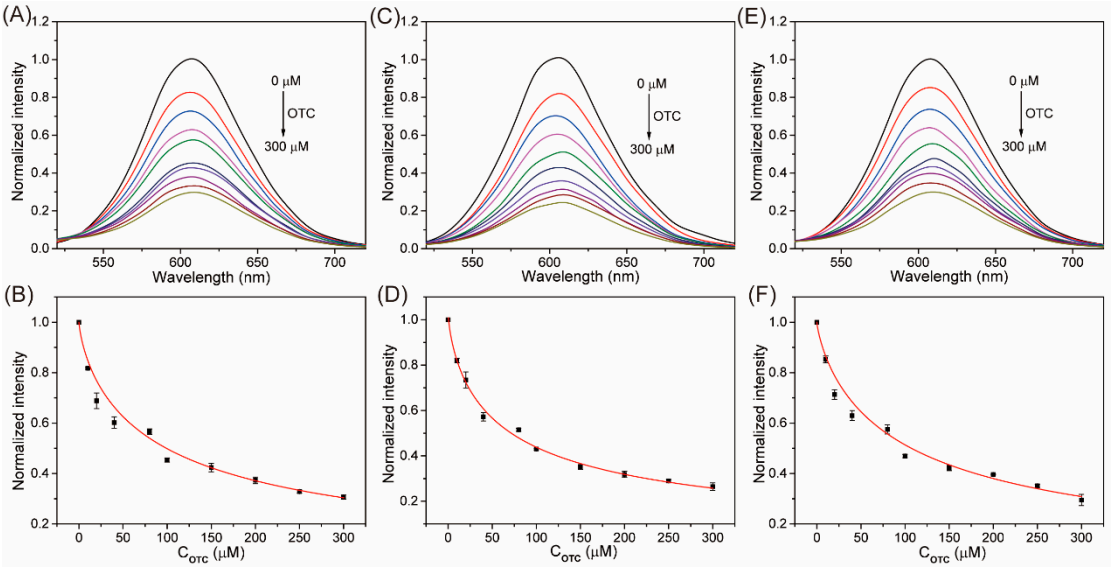

Figure S2. The fluorescence spectra of (A) MUA-AuNCs-Gd^{3+}, (C) MUA-AuNCs-$Ce^{3+}$and (E) MUA-AuNCs-Tm^{3+} towards OTC (0-300 μM). The changes of the normalized fluorescence intensity of (B) MUA-AuNCs-Gd^{3+}, (D) MUA-AuNCs-$Ce^{3+}$and (F) MUA-AuNCs-Tm^{3+} at 610 nm with the concentration of OTC (λ_{ex} = 265 nm).

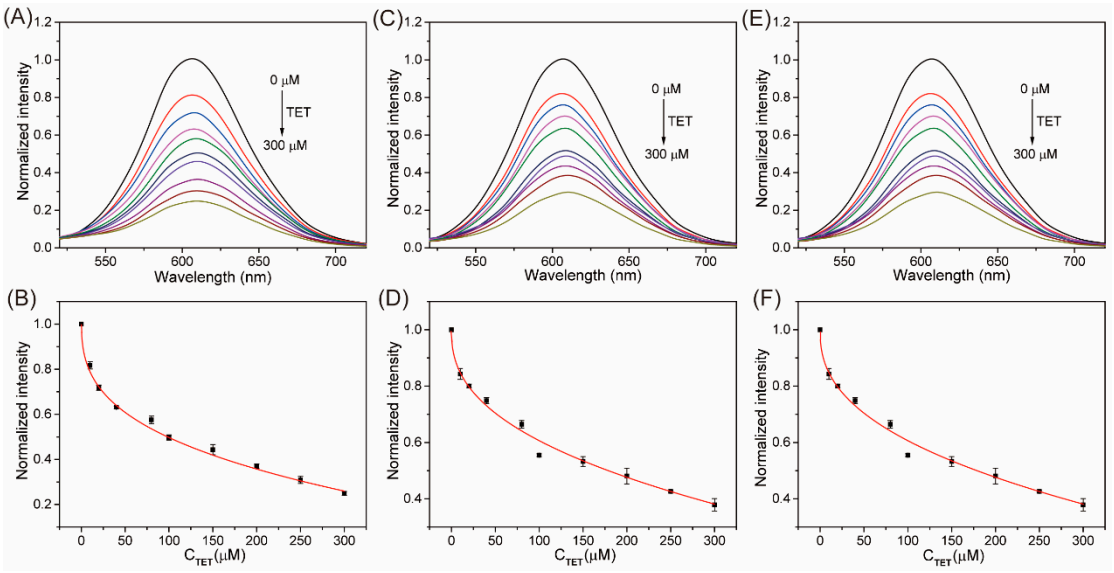

Figure S3. The fluorescence spectra of (A) MUA-AuNCs-Gd^{3+}, (C) MUA-AuNCs-$Ce^{3+}$and (E) MUA-AuNCs-Tm^{3+} towards TET (0-300 μM). The changes of the normalized fluorescence intensity of (B) MUA-AuNCs-Gd^{3+}, (D) MUA-AuNCs-$Ce^{3+}$and (F) MUA-AuNCs-Tm^{3+} at 610 nm with the concentration of TET (λ_{ex} = 265 nm).

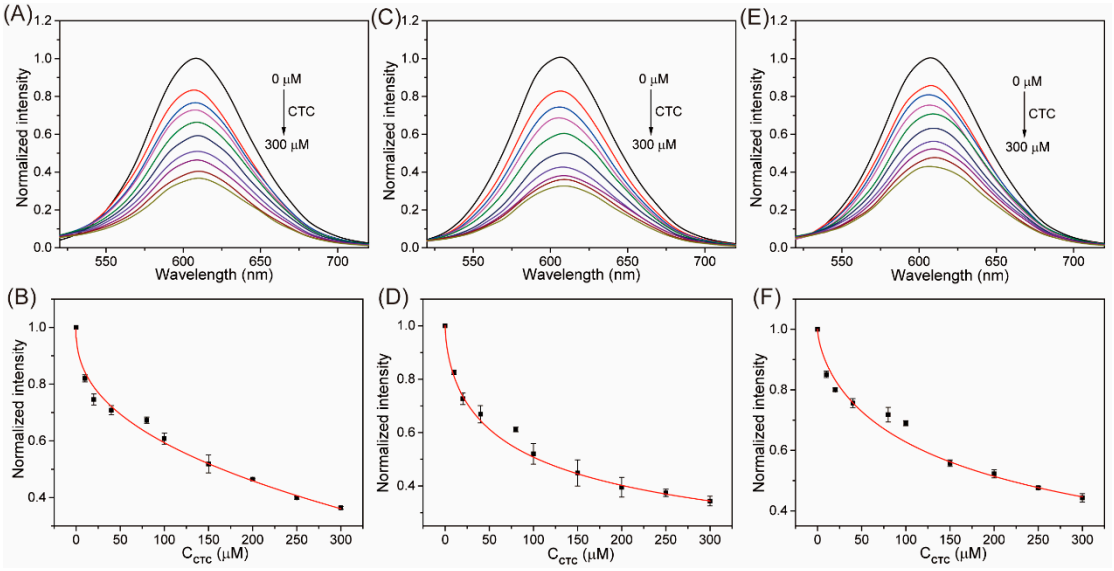

Figure S4. The fluorescence spectra of (A) MUA-AuNCs-Gd^{3+}, (C) MUA-AuNCs-$Ce^{3+}$and (E) MUA-AuNCs-Tm^{3+} towards CTC (0-300 μM). The changes of the normalized fluorescence intensity of (B) MUA-AuNCs-Gd^{3+}, (D) MUA-AuNCs-$Ce^{3+}$and (F) MUA-AuNCs-Tm^{3+} at 610 nm with the concentration of CTC (λ_{ex} = 265 nm).

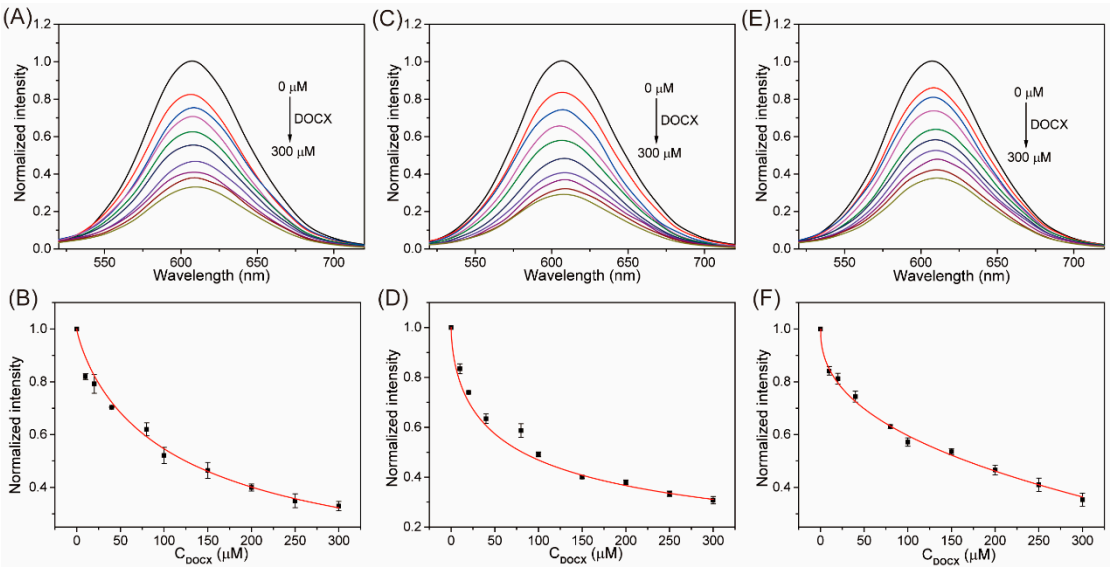

Figure S5. The fluorescence spectra of (A) MUA-AuNCs-Gd^{3+}, (C) MUA-AuNCs-$Ce^{3+}$and (E) MUA-AuNCs-Tm^{3+} towards DOCX (0-300 μM). The changes of the normalized fluorescence intensity of (B) MUA-AuNCs-Gd^{3+}, (D) MUA-AuNCs-$Ce^{3+}$and (F) MUA-AuNCs-Tm^{3+} at 610 nm with the concentration of DOCX (λ_{ex} = 265 nm).

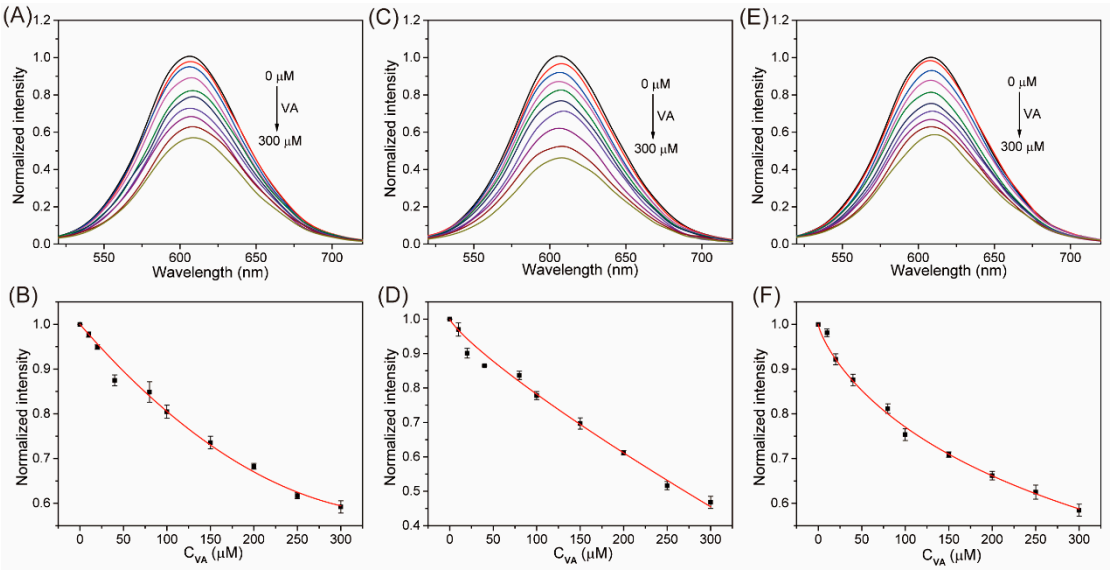

Figure S6. The fluorescence spectra of (A) MUA-AuNCs-Gd^{3+}, (C) MUA-AuNCs-$Ce^{3+}$and (E) MUA-AuNCs-Tm^{3+} towards VA (0-300 μM). The changes of the normalized fluorescence intensity of (B) MUA-AuNCs-Gd^{3+}, (D) MUA-AuNCs-$Ce^{3+}$and (F) MUA-AuNCs-Tm^{3+} at 610 nm with the concentration of VA (λ_{ex} = 265 nm).

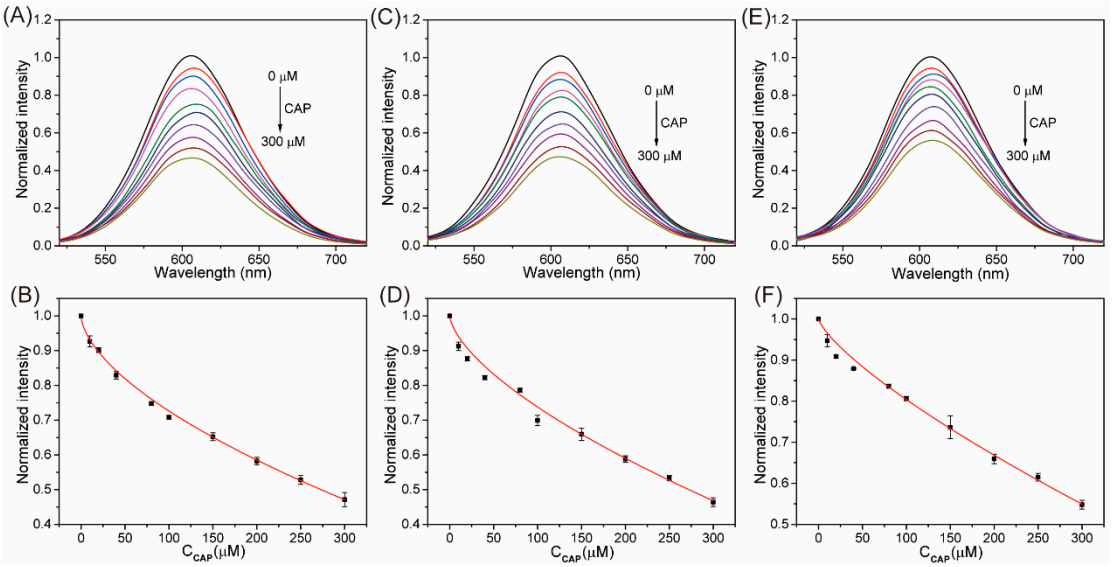

Figure S7. The fluorescence spectra of (A) MUA-AuNCs-Gd^{3+}, (C) MUA-AuNCs-$Ce^{3+}$and (E) MUA-AuNCs-Tm^{3+} towards CAP (0-300 μM). The changes of the normalized fluorescence intensity of (B) MUA-AuNCs-Gd^{3+}, (D) MUA-AuNCs-$Ce^{3+}$and (F) MUA-AuNCs-Tm^{3+} at 610 nm with the concentration of CAP (λ_{ex} = 265 nm).

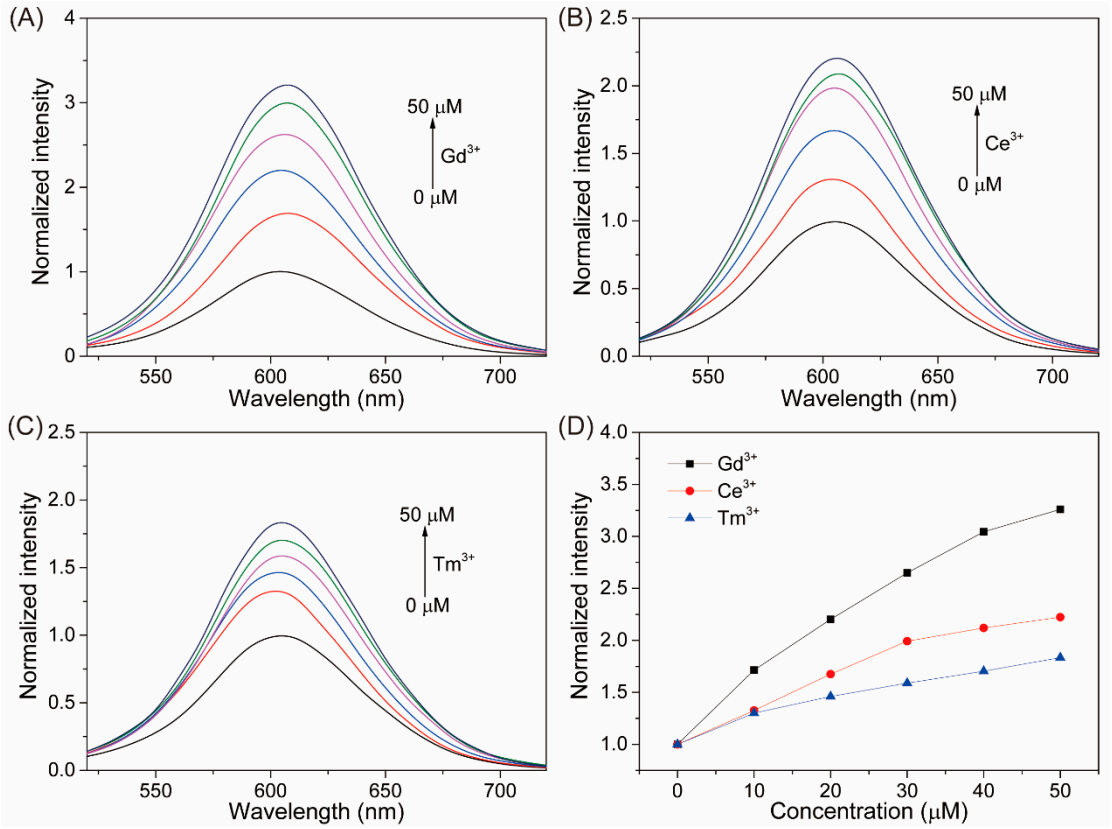

Figure S8. The effect of the concentration of the different rare earth ions on the fluorescence intensity of MUA-AuNCs. Fluorescence emission spectra of MUA-AuNCs after the addition of (A) Gd^{3+}, (B) Ce^{3+} and (C) Tm^{3+} (0-50 μM) in the pure aqueous solution (pH = 7.2). (D) The effect of the rare earth ions (0-50 μM) on the fluorescence intensity of MUA-AuNCs at 610 nm. (λ_{ex} = 265 nm).

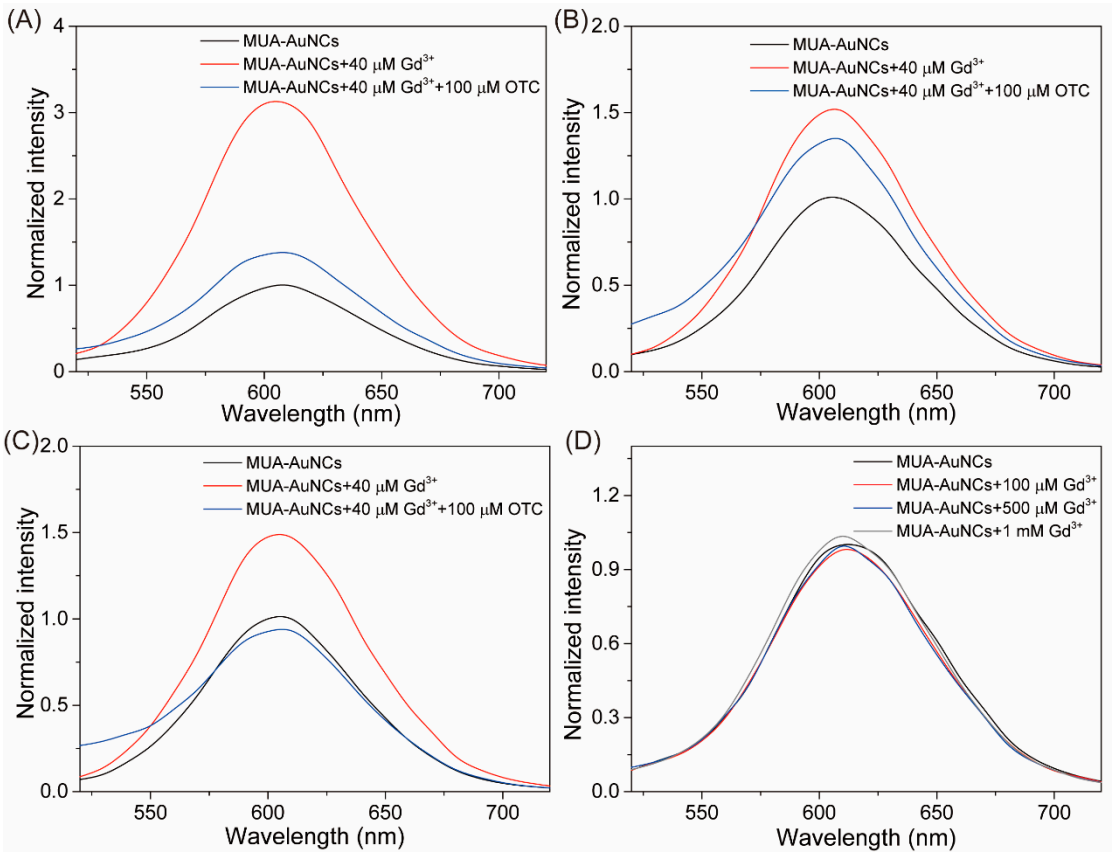

Figure S9. Fluorescence emission spectra of MUA-AuNCs-Gd^{3+} in different solutions in response to OTC. (A) Pure aqueous solution (pH = 7.2), (B) Tris-HCl solution (pH = 7.4), (C) HEPES buffer solution (pH = 7.4) and (D) PBS (pH = 7.4).

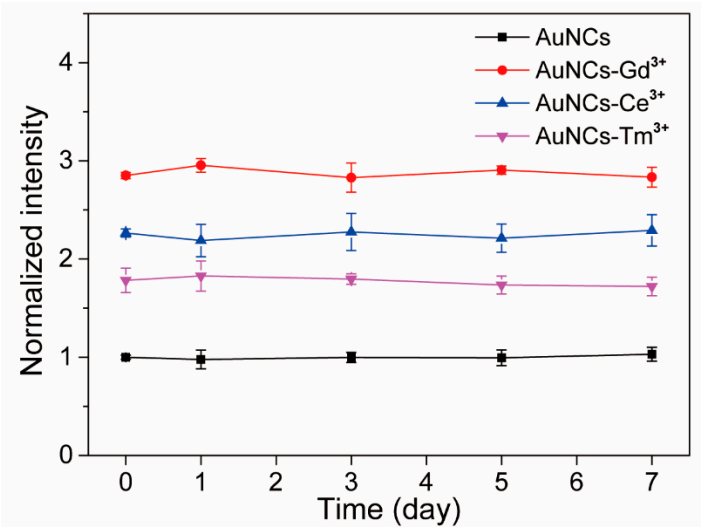

Figure S10. Fluorescence stability of MUA-AuNCs and different MUA-AuNCs-Re^{3+} within one week.

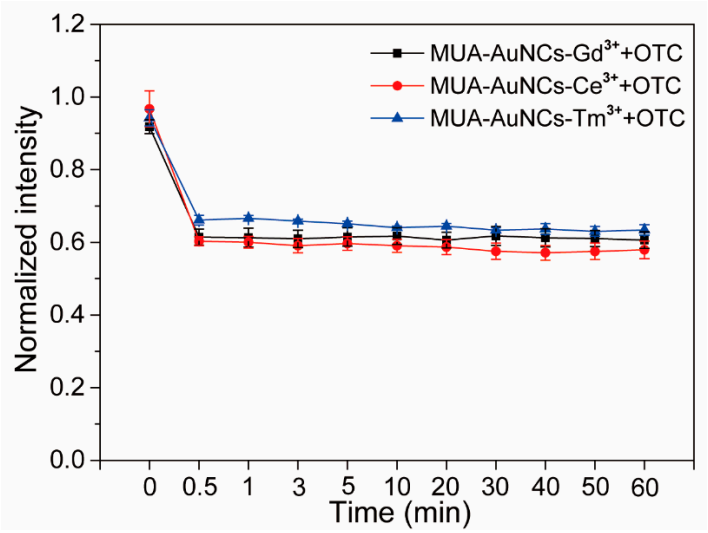

Figure S11. The effect of the response time with OTC on the fluorescence intensity of the MUA-AuNCs-Re^{3+} sensor array within 1 h (based on the normalized fluorescence intensity at 610 nm).

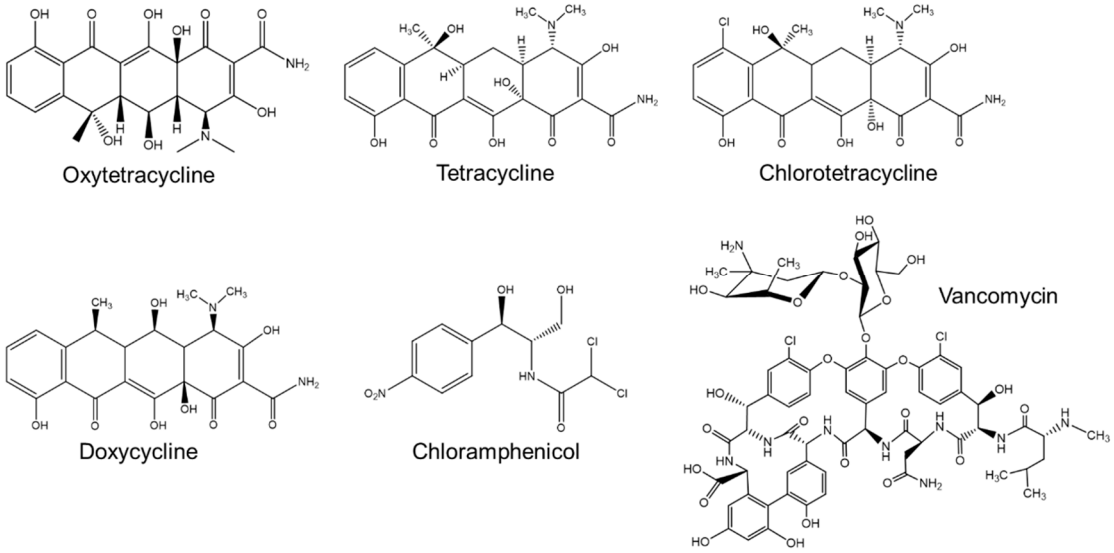

Figure S12. Chemical formulae of different antibiotics.

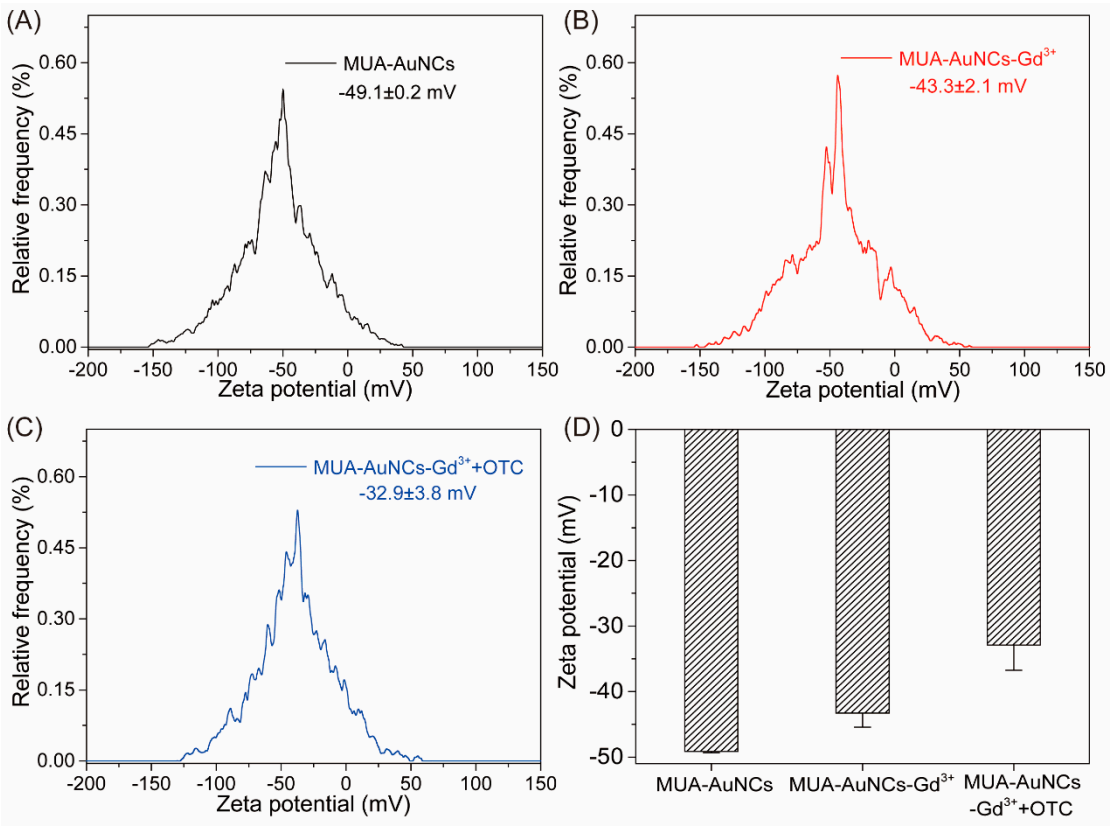

Figure S13. Zeta potential maps of (A) MUA-AuNCs, (B) MUA-AuNCs-Gd^{3+} and (C) MUA-AuNCs-Gd^{3+}+OTC. (D) Zeta potential of MUA-AuNCs after mixed with Gd^{3+} and OTC.

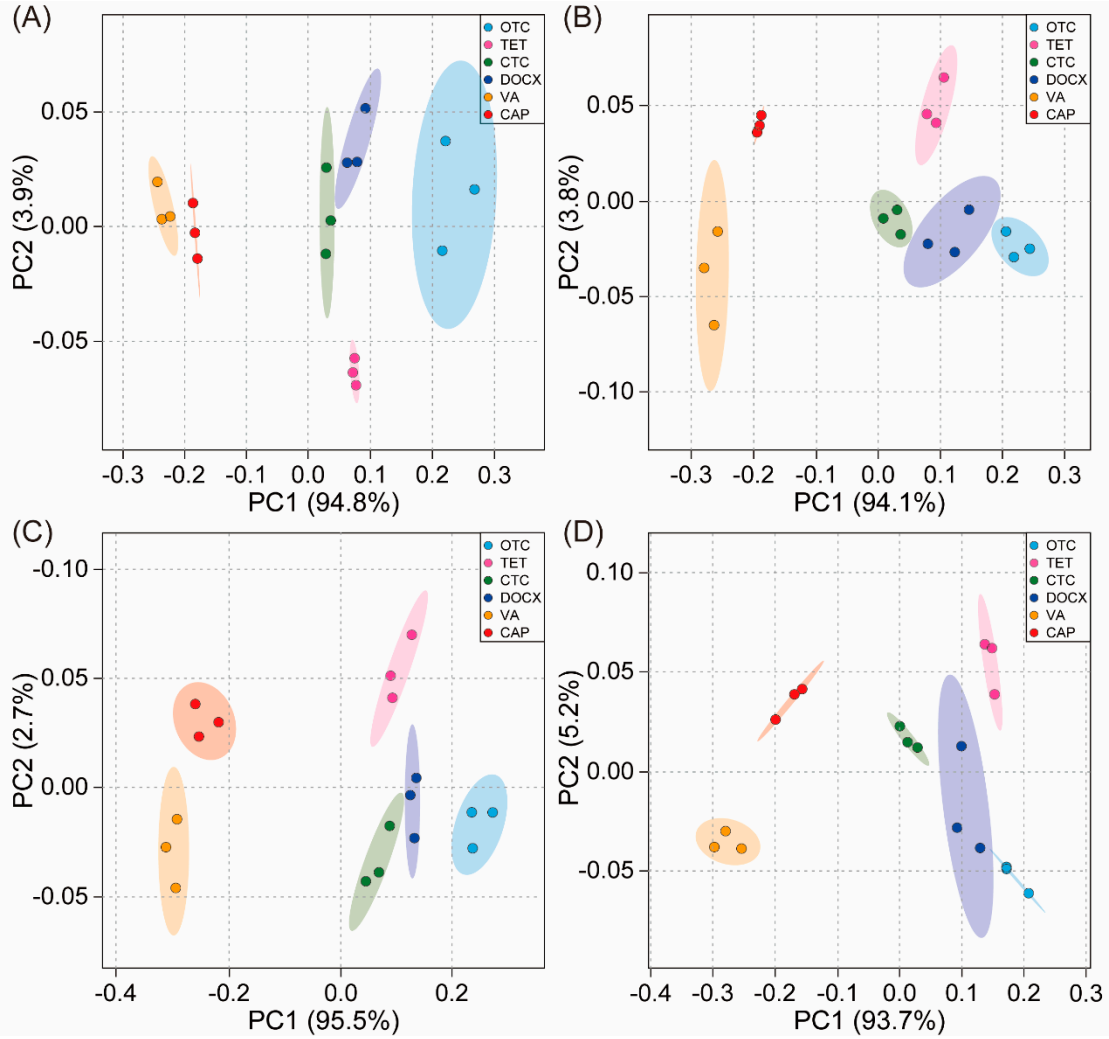

Figure S14. 2D PCA plots for the distinguish of the multiple antibiotics at different concentrations (A) 40 μM, (B) 80 μM, (C) 150 μM, and (D) 300 μM. The ellipses in the figure are plotted with 95% confidence intervals.

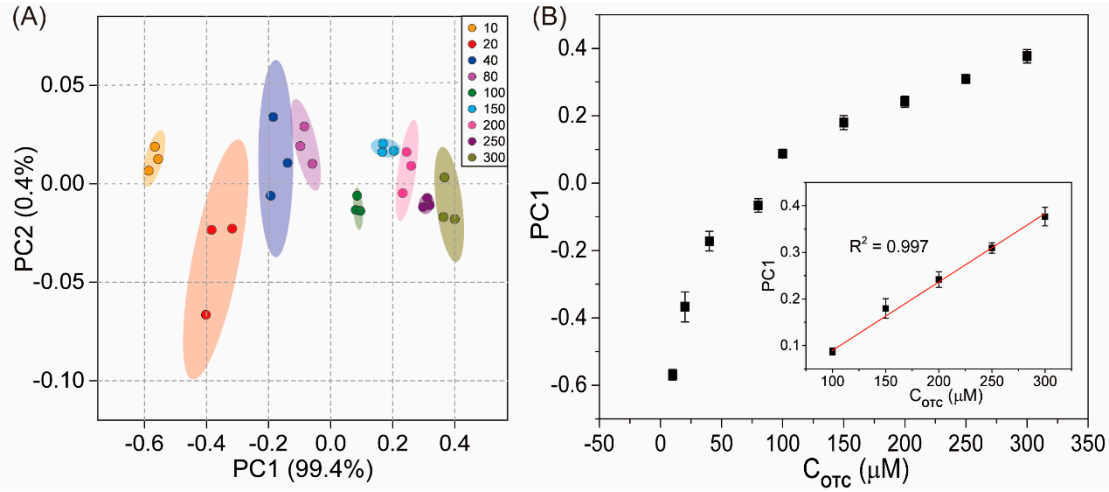

Figure S15. (A) 2D PCA plot of the MUA-AuNCs-Re^{3+} sensor array towards different concentrations of OTC (10-300 μM) (ellipses are drawn with 95% confidence). (B) PC1 of the sensor array plotted versus different concentrations of OTC. Inset: the linear relationship in the concentration of OTC from 100 to 300 μM (n = 3).

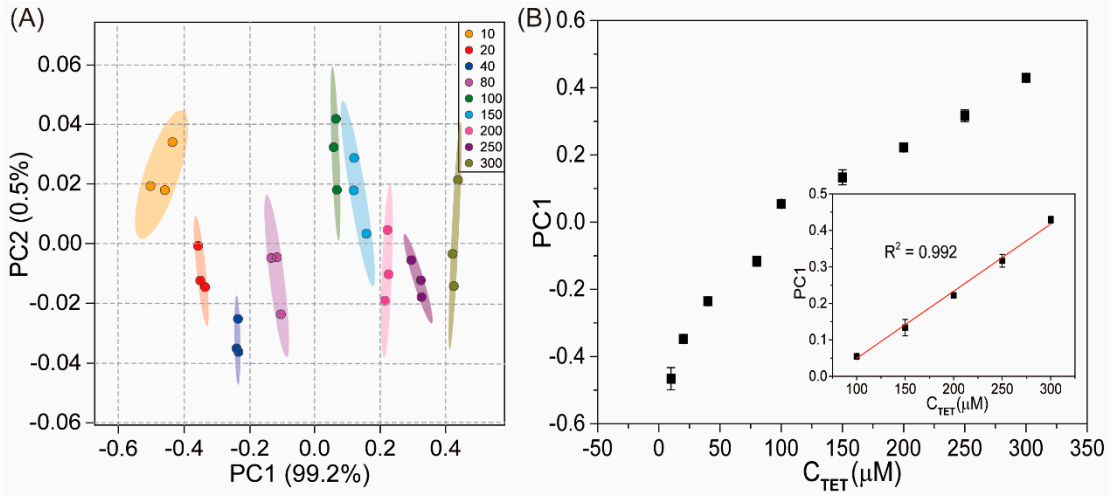

Figure S16. (A) 2D PCA plot of the MUA-AuNCs-Re^{3+} sensor array towards different concentrations of TET (10-300 μM) (ellipses are drawn with 95% confidence). (B) PC1 of the sensor array plotted versus different concentrations of TET. Inset: the linear relationship in the concentration of TET from 100 to 300 μM (n = 3).

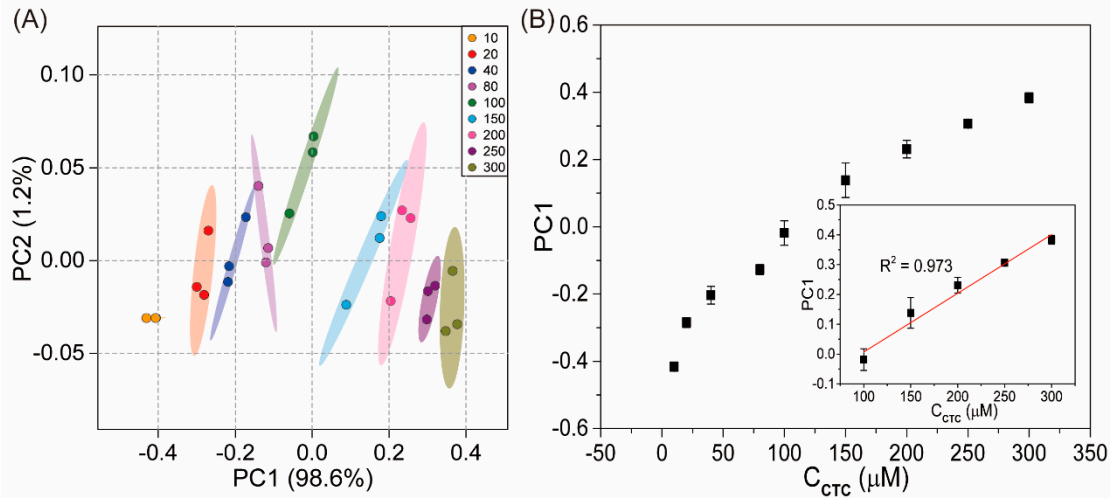

Figure S17. (A) 2D PCA plot of the MUA-AuNCs-Re^{3+} sensor array towards different concentrations of CTC (10-300 μM) (ellipses are drawn with 95% confidence). (B) PC1 of the sensor array plotted versus different concentrations of CTC. Inset: the linear relationship in the concentration of CTC from 100 to 300 μM (n = 3).

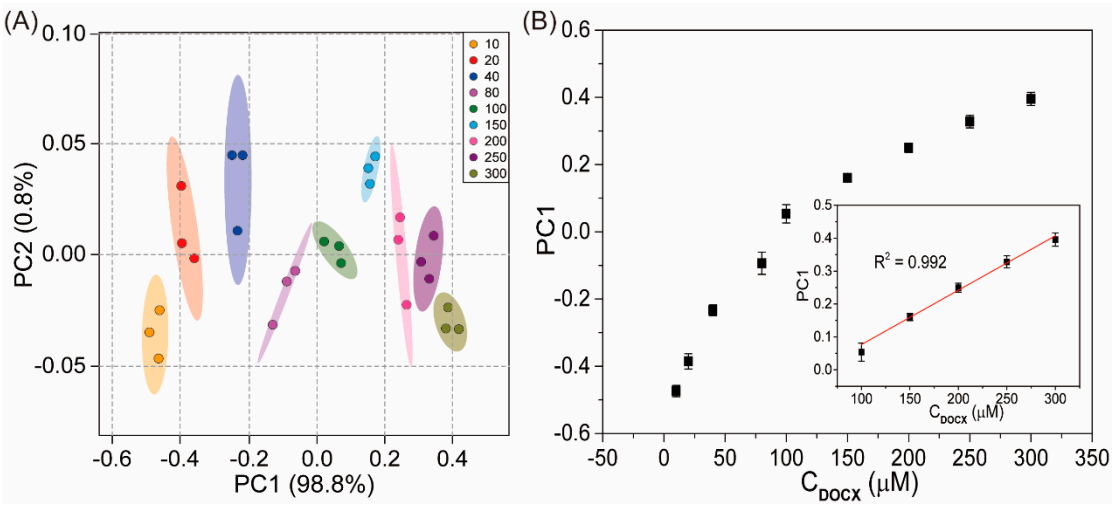

Figure S18. (A) 2D PCA plot of the MUA-AuNCs-Re^{3+} sensor array towards different concentrations of DOCX (10-300 μM) (ellipses are drawn with 95% confidence). (B) PC1 of the sensor array plotted versus different concentrations of DOCX. Inset: the linear relationship in the concentration of DOCX from 100 to 300 μM (n = 3).

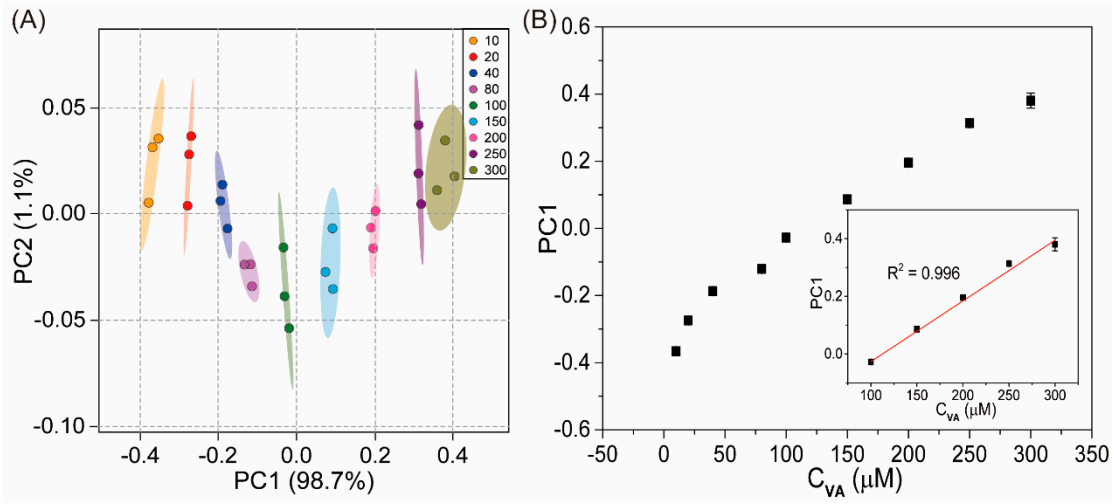

Figure S19. (A) 2D PCA plot of the MUA-AuNCs-Re^{3+} sensor array towards different concentrations of VA (10-300 μM) (ellipses are drawn with 95% confidence). (B) PC1 of the sensor array plotted versus different concentrations of VA Inset: the linear relationship in the concentration of VA from 100 to 300 μM (n = 3).

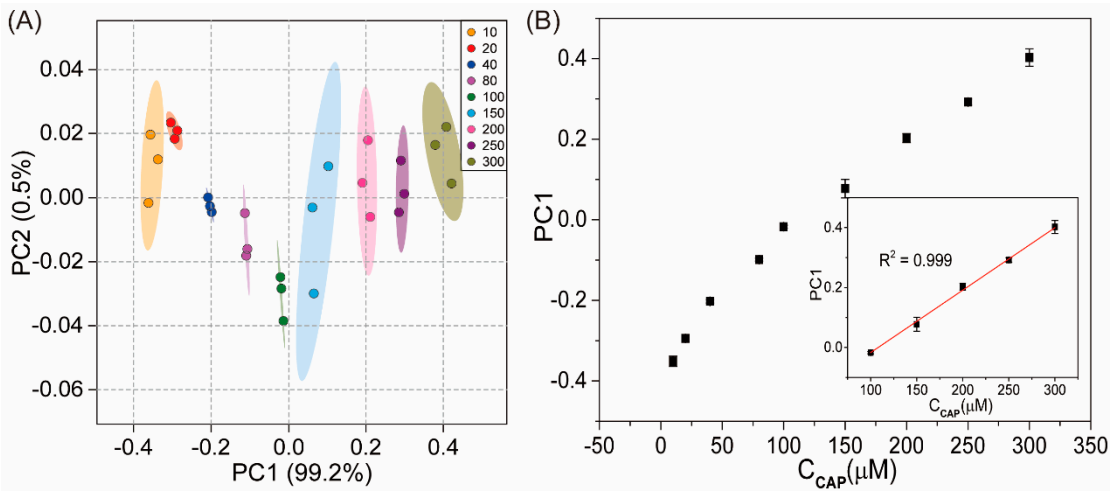

Figure S20. (A) 2D PCA plot of the MUA-AuNCs-Re^{3+} sensor array towards different concentrations of CAP (10-300 μM) (ellipses are drawn with 95% confidence). (B) PC1 of the sensor array plotted versus different concentrations of CAP. Inset: the linear relationship in the concentration of CAP from 100 to 300 μM (n = 3).